Materials Physics and Mechanics 42 (2019) 40-53 Received: October 6, 2018

THE INFLUENCE OF AN ADHESIVE LAYER ON THE INTERACTION BETWEEN A PIEZO-ACTUATOR AND AN ELASTIC 3D-LAYER AND ON THE EXCITED WAVE FIELDS

E.V. Kirillova[1], W. Seemann[2], M.S. Shevtsova[1,2*]

[1]RheinMain University of Applied Sciences, Wiesbaden, Germany

[2]Karlsruhe Institute of Technology, Karlsruhe, Germany

*e-mail: maria.shevtsova@hs-rm.de

Abstract. Piezoceramic transducers are extensively used in nondestructive testing (NDT), structural health monitoring (SHM) and condition monitoring (CM) of various mechanical systems including wind turbines, aircraft structures, bridges and pipeline systems. Piezoelectric transducers are surface bonded on the host structure and are excited to produce structural responses. This article highlights the effect of the adhesive layer between the studied structure and the transducer on the contact characteristics and the structural wave fields. The research also focuses on the efficiency of the both methods used for calculation of the occuring wave fields: finite-element (FE) method and semi-analytical approach based on the Green's matrix representations and the Fourier transform.

Keywords: anisotropic infinite layer, Green's matrix, piezoelectric actuator, wave excitation, finite element model, Fourier transform

1. Introduction

The condition monitoring (CM) of functional and safety-relevant components is an urgent requirement in different industrial sectors [1,2]. Condition monitoring allows one to mitigate risk, boost safety, and reduce maintenance costs for dynamically loaded components and systems. Compared to traditional non-destructive testing [3], where a more or less regular but timely inspection of the component takes place, in the CM the sensors remain permanently on or in the structure to be monitored and are polled on a permanent or periodic base. As a result, occurring damage can be detected by changes in the sensor signal almost immediately. Structural Health Monitoring [4–7] enables condition-based maintenance, increasing safety.

For integrated structural monitoring the ultrasonic waves in the form of Lamb waves represent a promising approach [8–12] since they appear merely in plate and shell structures, propagate over long distances and have a high sensitivity to detect damage. In order to use Lamb waves for damage detection in terms of active and integrated structural monitoring, special systems of sensors and actuators are required for excitation, reading and interpretation of the waves [11–18]. The actuators and sensors should be designed as surface transducers and are stated at the surface of the structure. Numerous studies assume an ideal contact between transducer and studied structure, however the effect of the bonding layer is described only in a few works [10,11,19–21]. This idealized assumption is not robust enough for structural monitoring since the transducers are always connected to the plate structure via an adhesive bonding layer. The adhesive layer transmits the forces between transducer and structure by mean shear stress. Due to its elastic properties, the power transmission is not ideal and is associated with losses. These losses are summarized in the literature under the

http://dx.doi.org/10.18720/MPM.4212019_5

term shear lag. Giurgiutiu in [6] proposes a model of mode transfer behaviour, which takes into account the influence of the adhesive layer on the shear force. A few studies [16–19,21] have been devoted to the effects of adhesive layers between surface-mounted PZTs and host structures for very low excitation frequencies up to several kHz, which corresponds to much bigger wavelengths compared to the size of the PZT. The shear lag effect [16] becomes more dominant with a lower shear modulus and thicker adhesive layer, and shear transfer between the PZT and host structure becomes less effective. In [11] effects of the adhesive bond-line layer on the Lamb wave generation and reception were simulated and compared with the available test data. It has been experimentally demonstrated in this article that the signal increases in amplitude as the thickness of the adhesive layer increases from 10 to 40 μm. It is explained by the fact that the resonance phenomenon of the PZT with a thicker and softer adhesive layer is less restricted, so that more energy could be generated from the PZT excitation. The study of the effect of adhesive layer remains a live issue and will be investigated.

The aim of this paper is to assess the need for using an adhesive layer between the host structure and piezoelectric element for modelling the wave propagation. With this purpose the dependence of the contact stresses and displacements on the characteristics of adhesive layer are analysed in the first part of the current study. Then the effect of taking into account this layer on the wave propagation in the isotropic and anisotropic layers is examined. These simulations are carried out using the FE-package Comsol Multiphysics at different vibration frequencies. The second part of the paper is devoted to comparing the results obtained for the FE- and the semi-analytical model, based on the Fourier transform, the Green's matrix representation [8,13] and the numerical contour integration.

2. Problem formulation

An infinite layer of thickness h is considered, which occupies the volume $D = \{(x, y, z) | -\infty < x < \infty; -\infty < y < \infty; -h \le z \le 0\}$. a The oscillations of the layer are excited by a PZT-actuator of thickness h_{PZT} and radius a, mounted on the upper surface of the host structure as shown in the Fig. 1. The thickness of the adhesive layer between the structure and the piezoelectric tablet is h_b. Time dependency is assumed harmonic in the form $e^{-i\omega t}$, where ω is the vibration frequency.

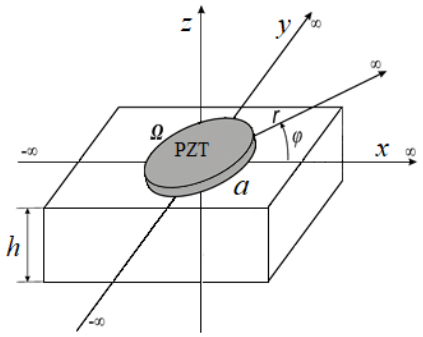

Fig. 1. Scheme of the loaded structure

Lame's equations for the steady-state harmonic vibrations of the layer are written in compact form:

$$L\mathbf{u} + \rho\omega^2\mathbf{u} = 0, \tag{1}$$

where ρ is the mass density and **u** is the displacement field. The upper and bottom surfaces of the layer are free of stress. The displacements **u** are caused by harmonic vibrations of a piezoelectric patch driven by a harmonically oscillating potential applied to the upper and

lower surfaces of the piezoelectric actuator. The fundamental equations of the PZT-actuator are represented in strain-charge form:

$$\boldsymbol{\varepsilon} = \mathbf{s}^E \cdot \boldsymbol{\sigma} + \mathbf{d}^* \cdot \mathbf{E} \tag{2}$$

$$\mathbf{D} = \mathbf{d} \cdot \boldsymbol{\sigma} + \varepsilon_0 \boldsymbol{\varepsilon}_r^{\,\sigma} \cdot \mathbf{E}, \tag{3}$$

where $\boldsymbol{\sigma}$ is the stress tensor and $\boldsymbol{\varepsilon}$ is the strain tensor, $\mathbf{s}^E$ is the compliance tensor for constant electric field, $\mathbf{d}$ is the piezoelectric charge coefficients matrix, $\mathbf{E}$ is the electric-field vector, $\mathbf{D}$ is the electric charge displacement density, and $\boldsymbol{\varepsilon}_r^{\sigma}$ is the electric permittivity tensor, constant ε_0 is the electric permittivity of free space and "*" indicates transpose operation. The tensor $\boldsymbol{\varepsilon}$ and the vector $\mathbf{E}$ are expressed in terms of the displacements $\mathbf{u}$ and the electric potential φ respectively

$$\boldsymbol{\varepsilon} = \frac{1}{2}(\nabla \mathbf{u} + \nabla \mathbf{u}^*), \tag{4}$$

$$\mathbf{E} = -\nabla \varphi. \tag{5}$$

The first aim of this study is to determine the displacement fields $\mathbf{u}$ occurring in isotropic and anisotropic infinite layers and to estimate the influence of the adhesive layer properties on the resulting contact characteristics calculated for the FE-model. This model is considered in detail in the next section.

3. Finite Element Model

Let us consider two different finite-element models simulating the structures actuated by a circular piezoelectric wafer. In the first model an isotropic thin layer of thickness h=2 mm is actuated by a piezoelectric thin-film actuator of thickness h_{PZT}=0.2 mm and radius a=10 mm made of PZT-5H with the piezoelectric constant d_{31}=−265 mm/kV. Material properties of the host structure are taken as follows: mass density ρ=2500 kg/m^3, Poisson's ratio ν=0.33 and Young's modulus E=20 GPa.

According to the second model an anisotropic layer of thickness h=4 mm is made of carbon fibre reinforced plastic (CFRP) material T700 is driven by piezoelectric actuator of the thickness h_{PZT}=2.1 mm and radius a=25 mm. The piezoelectric constant of the PZT-4 material used in the actuator is d_{31}=−140 mm/kV. Mechanical properties of the host structure are given through the following engineering constants: E_1=127.6 GPa, E_2=11.3 GPa, E_3=11.3 GPa, G_{12}=5.97 GPa, G_{13}=5.97 GP*a*, G_{23}=3.75 GPa, Poisson's ratios ν_{12}= ν_{13}=0.3, ν_{23}=0.34 and material density ρ=1578 kg/m^3.

In both FE-models the piezoelectric actuators are bonded to the host structure using an adhesive layer with the following properties: mass density ρ=910 kg/m^3, Poisson's ratio ν_{23}=0.37 and Young's modulus E=1.02 GPa. Thickness of the bonding layer is taken to be h_b=50 μm.

In both considered models, an electric potential is applied on the top of the PZT actuator, while its bottom surface is grounded. The amplitude of the electric potential is taken U=100 V in case of the isotropic host structure, and U=400 V in the second model with anisotropic host structure. A perfectly matched layer (PML) simulates a reflectionless boundary condition. The outer edge of the PML is fixed. All other boundaries are assumed to be free.

Unknown wave-fields are obtained by the frequency response analysis in a wide frequency range. Calculations are performed for both models in case with and without a bonding layer.

4. Numerical results for the finite element model

Comparison of the contact characteristics for the models with and without bonding layer. Below in Fig. 2, contact shear stresses for the isotropic structure are presented depending on the glue thickness. The vibration frequencies are taken equal to f=15 kHz (a) and f=145 kHz (b). One can see that a thicker bonding layer with the thickness h_b=50 μm produces a weakened load transfer between the piezoelectric actuator and the host structure. In the model without bonding layer when h_b=0 μm the shear stresses are concentrated at the edge of the circular contact zone. Fig. 3 demonstrates the amplitudes of the r- components of contact displacements distribution, while the z-components are present in Fig. 4 at the vibration frequencies f=15 kHz (a) and f=145 kHz (b). It should be noticed that the use of a bonding layer leads to a smoother distribution of the displacements near the end of the contact zone. It is apparent that in the case of lower frequencies, the contact displacements can be approximated by a linear function. With the growth of the frequency, the distribution of contact characteristics has a more complicated character and cannot be approximated by well-known simple functions.

In Fig. 5, contact shear stresses for the anisotropic layer are present depending on the glue thickness and the angle γ. It is obvious that the influences of a bonding layer on the contact shear stresses and displacement fields are the same as for the isotropic structure. It should be noticed that the contact characteristics calculated for $\gamma = 0^\circ$, along the fibers, have significantly higher amplitudes than the characteristics obtained at $\gamma = 90^\circ$. Contact r-displacements presented in Fig. 6 have approximately three times higher amplitudes at $\gamma = 0^\circ$ (a) than at $\gamma = 90^\circ$ (b).

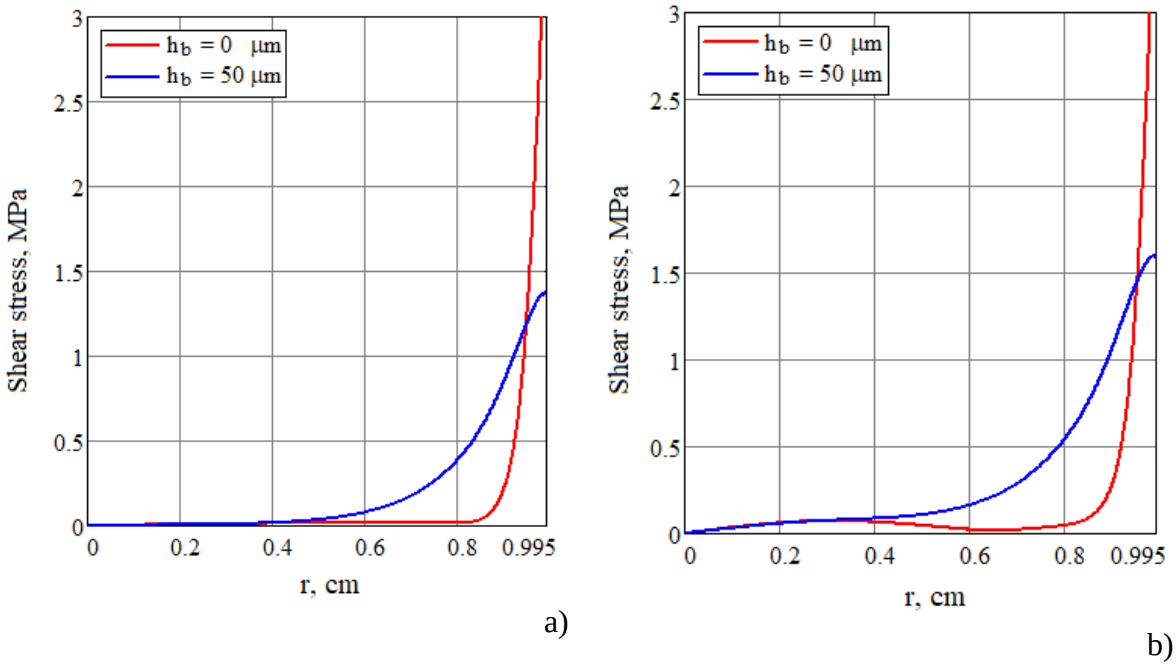

Fig. 2. Absolute values of contact shear stresses in an isotropic structure depending on the thickness of the bonding layer at f=15 kHz (a) and f=145 kHz (b)

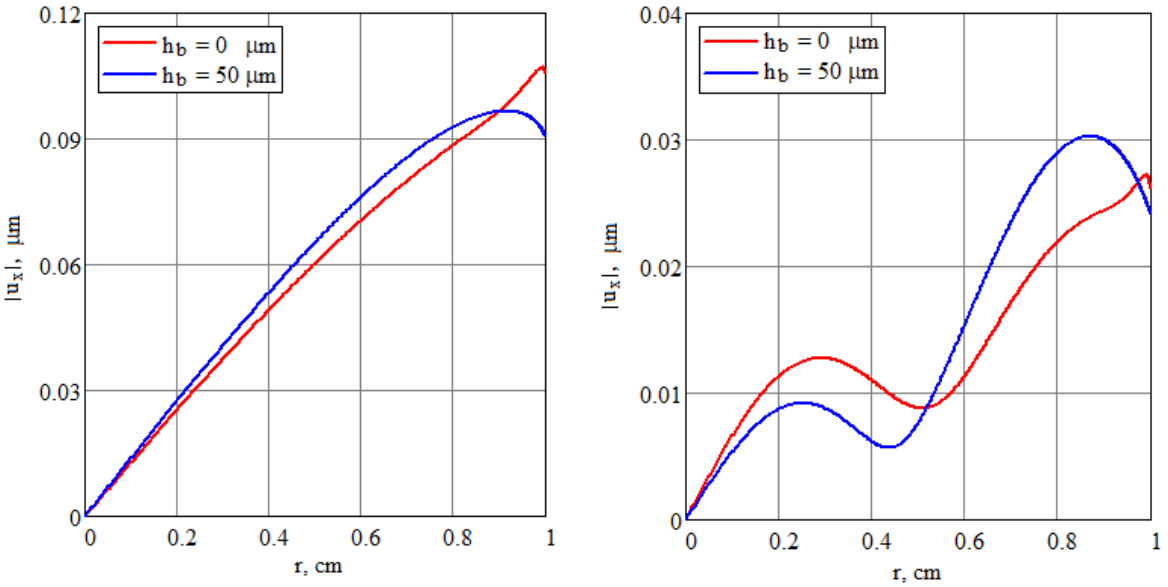

a) b)

Fig. 3. Absolute values of *r* -components of contact displacements in an isotropic structure depending on the thickness of the bonding layer at *f*=15 kHz (a) and *f*=145 kHz (b)

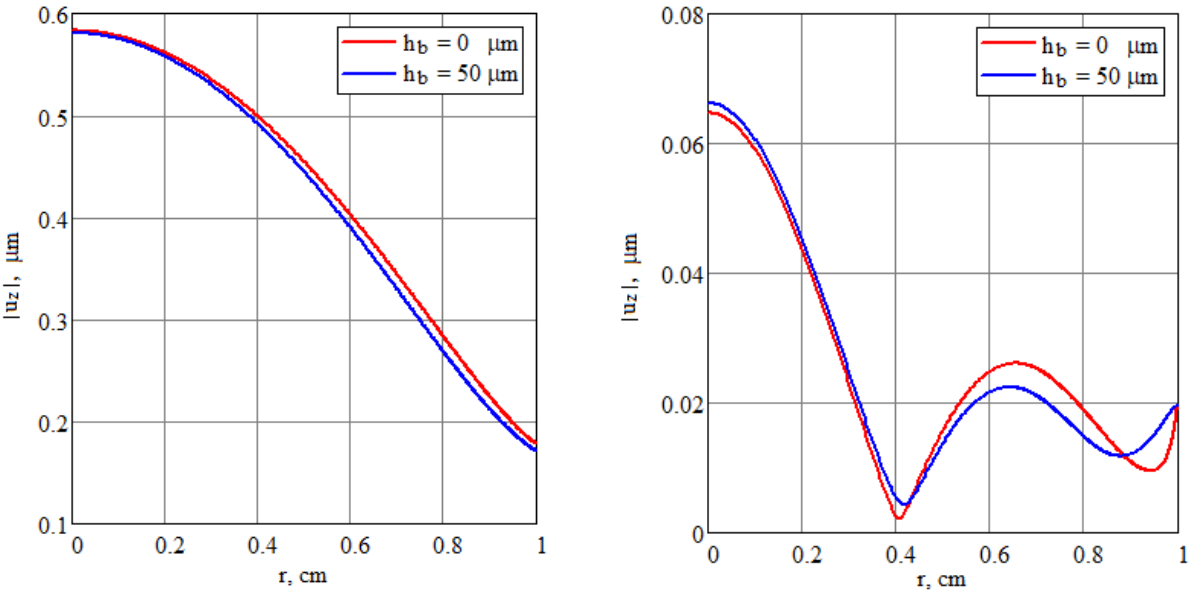

a) b)

Fig. 4. Absolute values of *z*-components of contact displacements in an isotropic structure depending on the thickness of the bonding layer at *f*=15 kHz (a) and *f*=145 kHz (b)

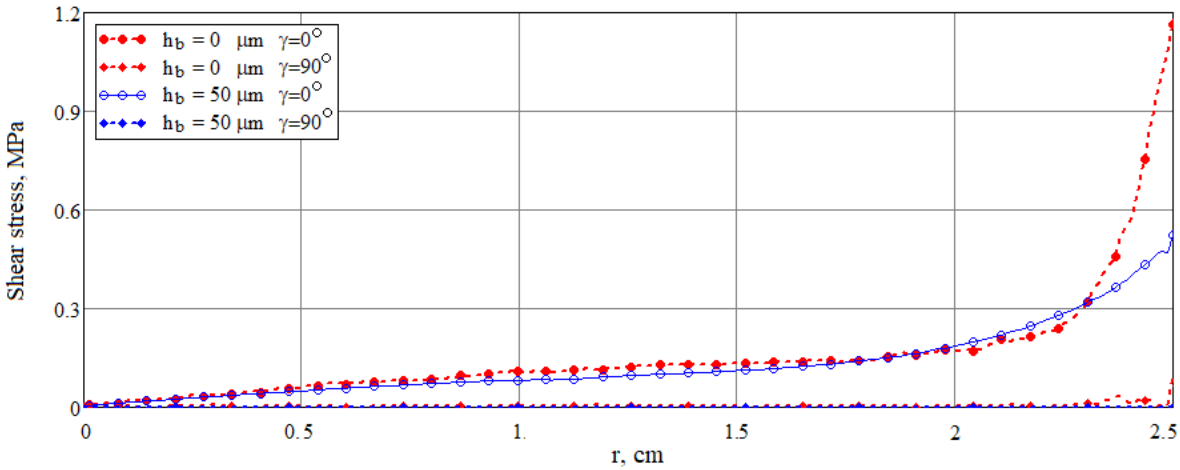

Fig. 5. Absolute values of contact shear stresses in an anisotropic structure depending on the bond thickness and angle γ at f=15 kHz

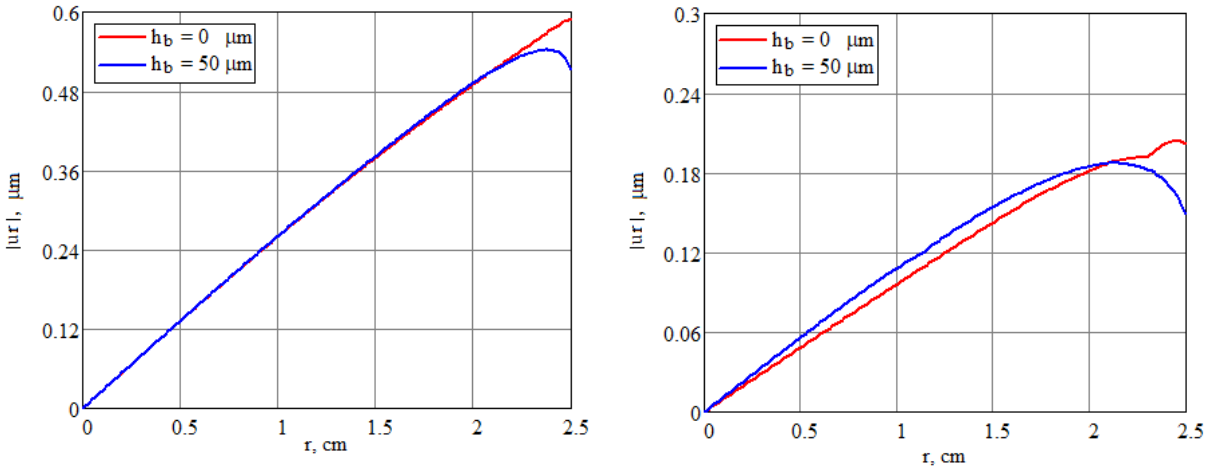

a) b)

Fig. 6. Absolute values of contact r-displacements in an anisotropic structure depending on the thickness of the bonding layer at $\gamma = 0^\circ$ (a) and $\gamma = 90^\circ$ (b) at f=15 kHz

Dependency of wave propagation on the adhesive layer characteristics.

Below the surface r- (a) and z- (b) displacements of the isotropic layer are presented at vibration frequency f=15 kHz (Fig.7) and f=145 kHz (Fig. 8). The results obtained for two models with and without bonding layer between the host structure and the PZT-actuator are compared. One can see that the bonding layer influences mostly the r-components of the surface displacements near the vibration source. The difference of displacement amplitudes in a far field is insignificant for both r- and z-components.

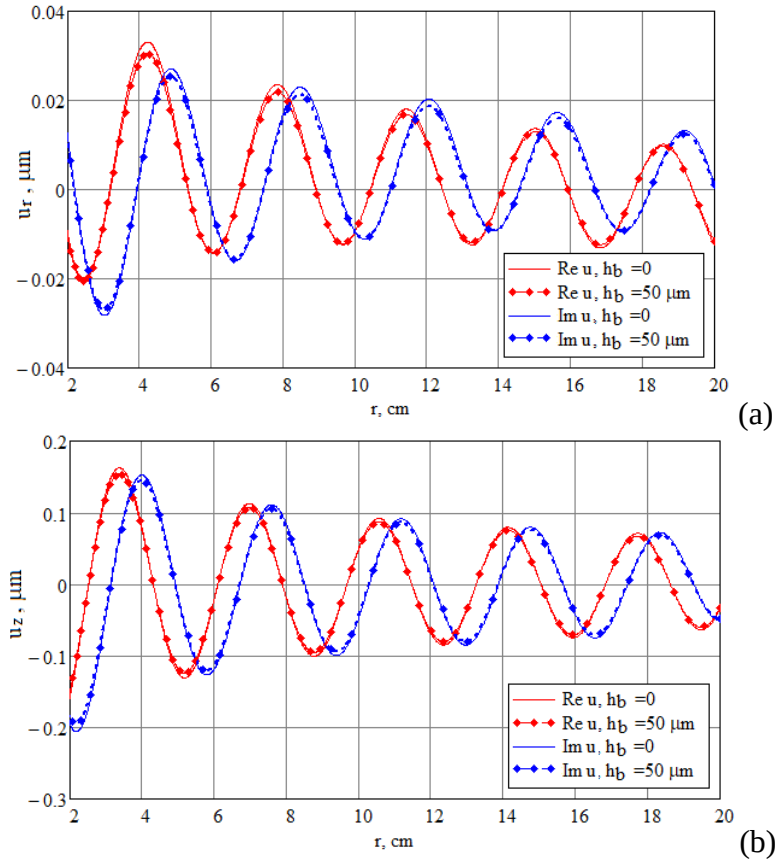

Fig. 7. Real and imaginary parts of surface *r*- (a) and *z*- (b) displacements for an isotropic plate depending on the bond thickness at *f*=15 kHz

Similar calculations were simulated for an anisotropic CFRP-plate. The comparison was performed at different directions: along the fibre direction at $\gamma = 0°$ and at $\gamma = 90°$ across the fibres. The surface *r*-displacements distribution of the anisotropic plate is present in Fig. 9, and Fig. 10 demonstrates *z*-displacements. In both figures wave fields are calculated at a vibration frequency *f*=10 kHz and the angles $\gamma = 0°$ (a) and $\gamma = 90°$ (b). It is obvious that similar to the isotropic structure case the influence of the bonding layer on the surface displacements is negligible in the far field. The amplitudes obtained for the model without bonding layer take higher values near the vibration source compared to the model with an adhesive layer.

It is apparent from the Fig. 9 that the amplitudes of surface *r*-displacements calculated along the fibers direction (a) take more than ten times higher values than the displacements in perpendicular direction (b). One can see from Fig. 10 that the *z*-components of displacements calculated across the fibers (a) have approximately five times lower values than the displacements along the composite fibers. This effect is clearly visible in Fig. 11, where the surface plot of the *z*-displacements at vibration frequency *f*=10 kHz is shown. In this figure the highest amplitudes are present in red color and it is visible that the oscillations propagate along the composite fibers from the vibration source placed in the middle of the host structure. They slightly attenuate along the host structure and approach zero values in the area of a perfectly matched layer.

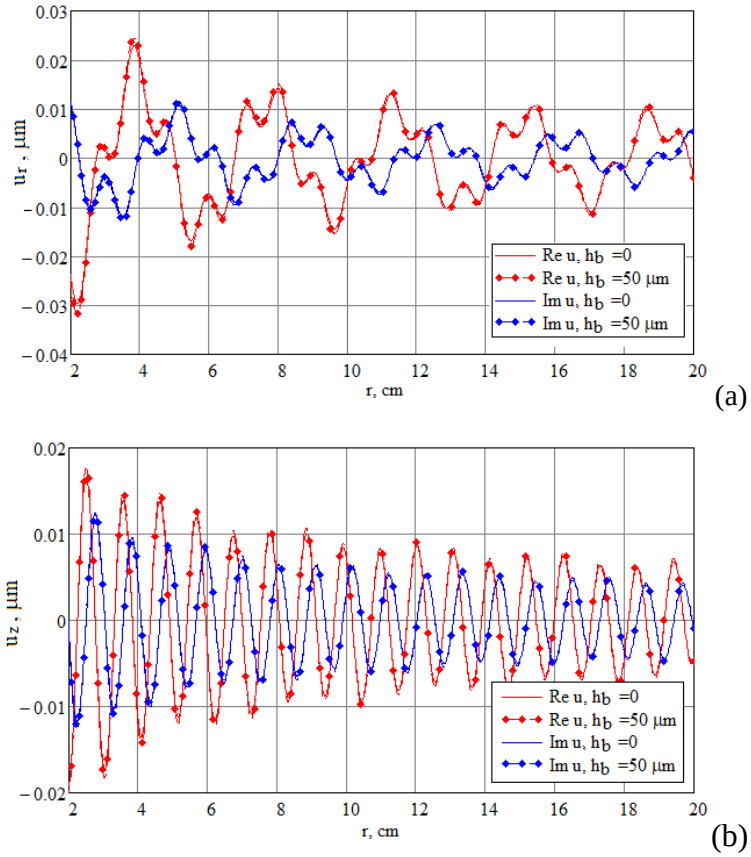

Fig. 8. Real and imaginary parts of surface *r*- (a) and *z*- (b) displacements for an isotropic plate depending on the bond thickness at f=145 kHz

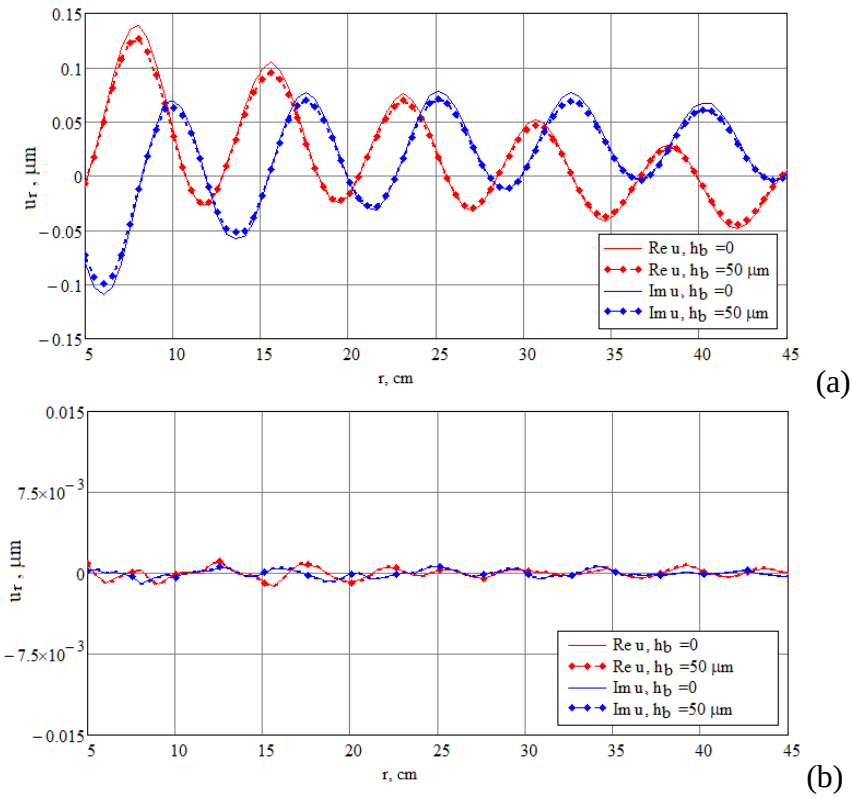

Fig. 9. Real and imaginary parts of surface *r*-displacement depending on the bond thickness at $\gamma = 0°$ (a) and $\gamma = 90°$ (b) at f=10 kHz

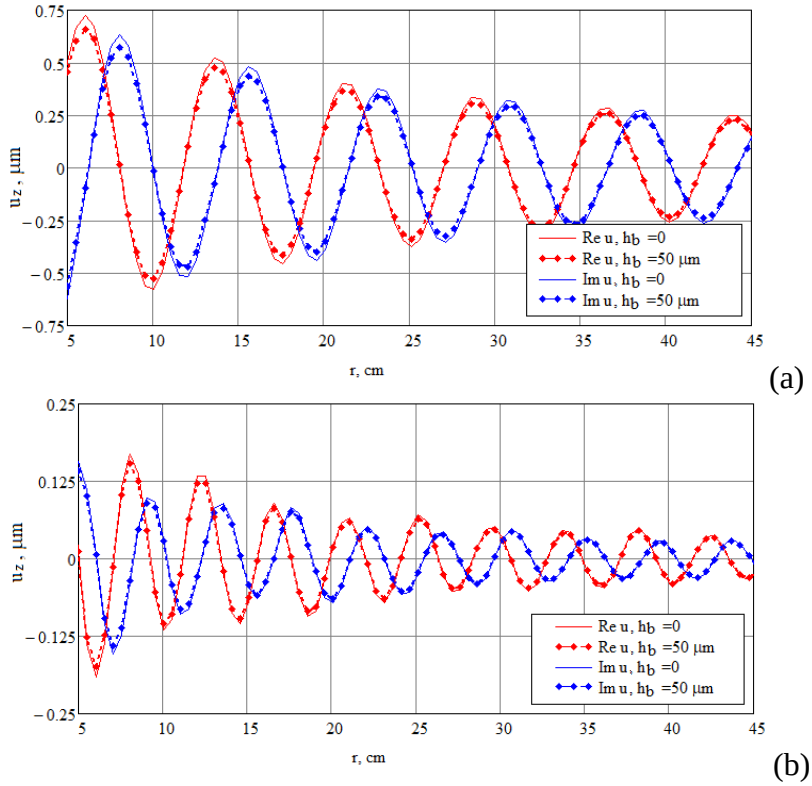

Fig. 10. Real and imaginary parts of surface *z*-displacement depending on the bond thickness at $\gamma = 0°$ (a) and $\gamma = 90°$ (b) at *f*=10 kHz

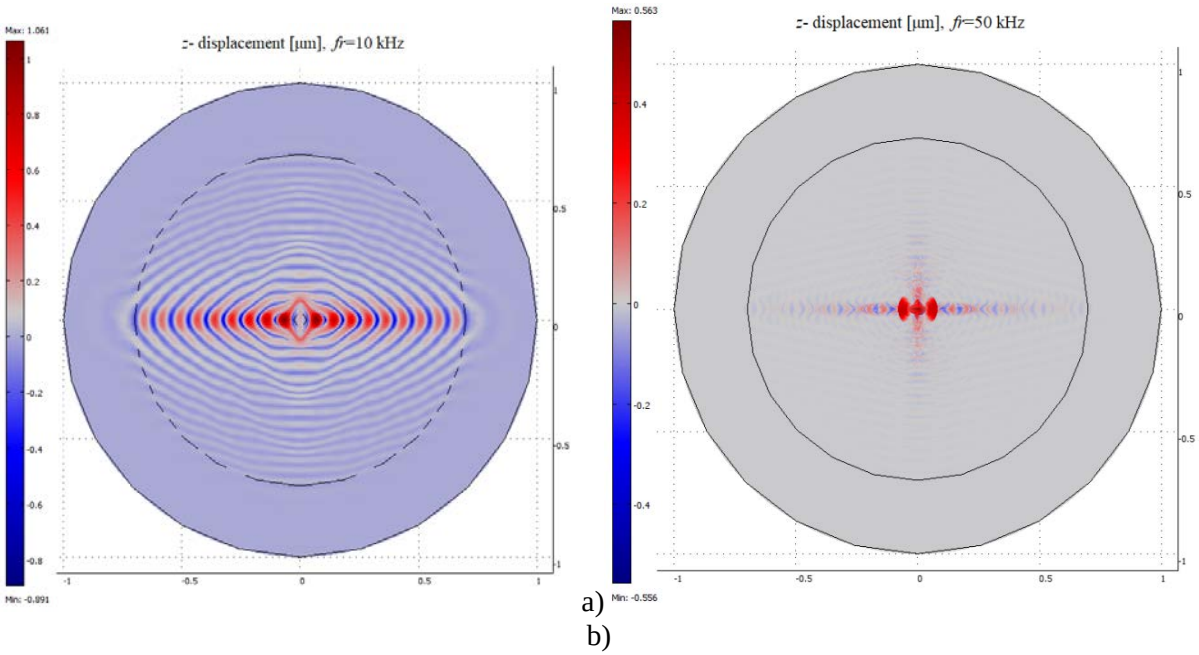

Fig. 11. Surface plots of *z*-displacement [μm] distribution in a carbon fiber plate at different vibration frequencies: *f*=10 kHz (a) and *f*=50 kHz (b)

5. Simulation of the wave field using Fourier transform

The second semi-analytical approach for the determination of wave fields appearing in isotropic or anisotropic infinite layers is based on an application of the Fourier transform and Green's matrix formulation. The Fourier transform with respect to the coordinates *x*, *y* is applied to the equation (1) and boundary conditions. The solution of the considered problem can be represented in the Fourier domain as follows [8]:

$$U_i(\alpha_1,\alpha_2,z)=K_{ij}(\alpha_1,\alpha_2,z)Q_j(\alpha_1,\alpha_2),\ i,j=\ 1,\ \ 2,\ \ 3, \tag{6}$$

where $K_{ij}(\alpha_1,\alpha_2,z)$ is the Fourier transform of the elements of Green's matrix **K** of the considered structure, and vector $\mathbf{Q}$ with the components $Q_j(\alpha_1,\alpha_2)$ is the Fourier transform of the load vector $\mathbf{q}(x,y)$. An algorithm to evaluate Green's matrix in the frequency-wavenumber domain is described in detail in [8]. In order to obtain the displacement vector **u**, the inverse Fourier transform to the vector **U** was applied:

$$\mathbf{u}(x,y,z)=\frac{1}{4\pi^2}\int_{\Gamma_1}\int_{\Gamma_2}\mathbf{K}(\alpha_1,\alpha_2,z)\mathbf{Q}(\alpha_1,\alpha_2)e^{-i(\alpha_1 x+\alpha_2 y)}d\alpha_1 d\alpha_2, \tag{7}$$

or in cylindrical coordinates

$$\mathbf{u}(r,\varphi,z)=\frac{1}{4\pi^2}\int_0^{2\pi}\int_{\Gamma^+(\gamma)}\mathbf{K}(\alpha,\gamma,z)\mathbf{Q}(\alpha,\gamma)e^{-i\alpha r\cos(\gamma-\varphi)}\alpha d\alpha d\gamma, \tag{8}$$

where $x=r\cos\varphi$, $y=r\sin\varphi$, $z=z$, $r=\sqrt{x^2+y^2}$, $\alpha_1=\alpha\cos\gamma$, $\alpha_2=\alpha\sin\gamma$ and $\alpha=\sqrt{\alpha_1^2+\alpha_2^2}$. Here $\gamma\in[0,2\pi]$ and $\varphi\in[0,2\pi]$ are assumed to be real, Γ_1, Γ_2, $\Gamma^+(\gamma)$ denote the integration contours, which partially deviate from the real axis while bypassing the real poles of the Green's functions in accordance with the principle of limiting absorption [22]. According to this principle, the integration contour Γ^+ bypasses positive real poles of the matrix **K** from below in case without backward waves (see Fig. 12).

In this work a computation of the displacements in an anisotropic plate caused by a circular PZT-actuator of radius r_0 using a semi-analytical procedure is present. The action of a circular source can be represented as follows

$$\tau_{xz}=\tau_0\delta(r-r_0)\cos\varphi,\ \tau_{yz}=\tau_0\delta(r-r_0)\sin\varphi,\ \sigma_z=0\ \text{ for } z=0. \tag{9}$$

The application of the double Fourier transform leads to

$$\begin{aligned}Q_1(\alpha,\gamma)&=2\pi i\tau_0 r_0 J_1(r_0\alpha)\cos\gamma,\\ Q_2(\alpha,\gamma)&=2\pi i\tau_0 r_0 J_1(r_0\alpha)\sin\gamma,\\ Q_3(\alpha,\gamma)&=0,\end{aligned} \tag{10}$$

where $J_1(r_0\alpha)$ is the Bessel function of the first kind. Surface displacements (8) are computed using the integral approach based on the Fourier transform after finding the solution of the problem in Fourier domain [8]. This requires the computation of the inverse Fourier transform, which means the computation of the two-dimensional improper contour integral and consecutive evaluation of the integral with respect to the frequency ω.

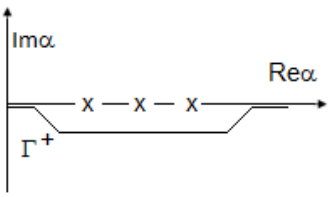

Fig. 12. Integration contour

The computation of the double integral (8) over wavenumbers causes such difficulties as integral singularity near real poles of Green's matrix, strong oscillations of the integrand and significant time expenses. The following sequence of double integrals can be considered:

$$\mathbf{u}_{R_n}(r,\varphi,z)=\frac{1}{4\pi^2}\int_0^{2\pi}\int_{\Gamma^+_{R_n}(\gamma)}\mathbf{K}(\alpha,\gamma,z)\mathbf{Q}(\alpha,\gamma)e^{-i\alpha r\cos(\gamma-\varphi)}\alpha d\alpha d\gamma\,, \tag{11}$$

where $\Gamma^+_{R_n}\to\Gamma^+$, $n\to\infty$. The sequence (11) converges to the initial 2D-integral, i.e. $\forall\varepsilon>0$, $\forall\omega,\varphi,z$, $\forall r>0$, $\exists n>0$:

$$\left|u_j(r,\varphi,z)-u_{j,R_n}(r,\varphi,z)\right|<\varepsilon,\quad j=1,2,3\,. \tag{12}$$

Thus instead of the improper double integral (8) the double integral over the bounded domain (11) can be considered, i.e. for a given value ε such $R = R_n$ exists that

$$\mathbf{u}(r,\varphi,z)\approx\mathbf{u}_R(r,\varphi,z)\,, \tag{13}$$

and (11) is satisfied. An example of a contour Γ^+_R in the case when all the real poles except the only one irregular pole $k_1(\gamma)$ are regular, is present in Fig.13.

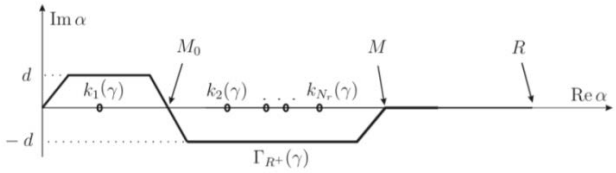

Fig. 13. Finite integration contour $\Gamma^+_{R_n}$

Here $d=\mathrm{Im}\,k_{nc}(\gamma)/2$ is the value of the deviation of the integration contour from the real axis into the complex plane, k_{nc} is the complex pole nearest to the real axis, $M=\max_m k_m(\gamma)$, k_m are real poles, and the value R is taken so that $M<\mathrm{Re}\,\alpha\le R$. For the evaluation of the 2D-wavenumber integral (8) as an iterated integral (11), the integration with adaptive quadratures [23] is applied in this work.

6. Comparison of surface displacements for FE- and semi-analytical models

An example of the calculation of displacement fields for the CFRP-panel of the thickness h=1 mm and material properties described in Section 3, is illustrated below. The harmonic wave propagation is excited by a load (9), distributed in a circle of radius R=2.5 mm at vibration frequencies f=10 kHz and f=40 kHz. The real and imaginary amplitudes of z-displacements are evaluated in direction $\gamma=0°$ using the semi-analytical and the FE-approaches. The results obtained for f=10 kHz are present in Fig. 14, and Fig. 15 corresponds to the vibration frequency f=40 kHz. It is obvious that both approaches give comparable results. The slight difference in the ampitudes is visible near the excitation source, whereas the results obtained in a far field agree well for both considered approaches. The best results agreement corresponds to the lower vibration frequency (Fig. 14). It should be noted that the higher frequency (Fig. 15) needs a sufficient computational cost due to the FE-mesh refinement and the consequently significant time costs, since the axial-symmetry model cannot be applied for an anistropic plate and the 3D-model is requiered. Thereby the required computation time for the FE-model increases with increasing frequency, whereas the semi-analytical approach works equally fast for any properties of a host-structure and at any vibration frequency.

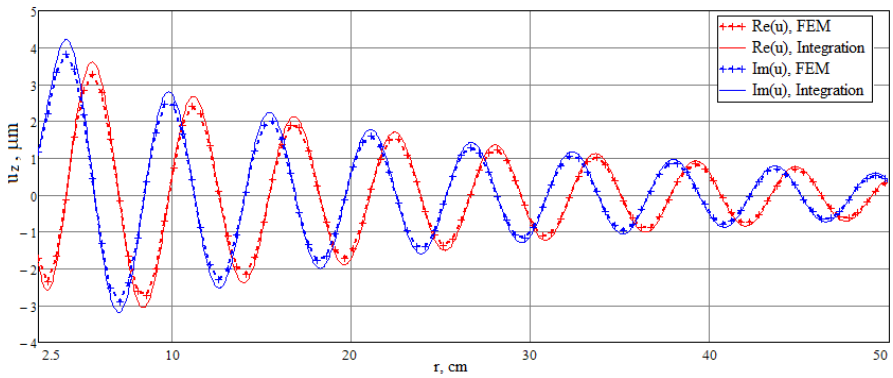

Fig. 14. Surface *z*-displacement of anisotropic plate at $\gamma = 0°$ and f=10 kHz

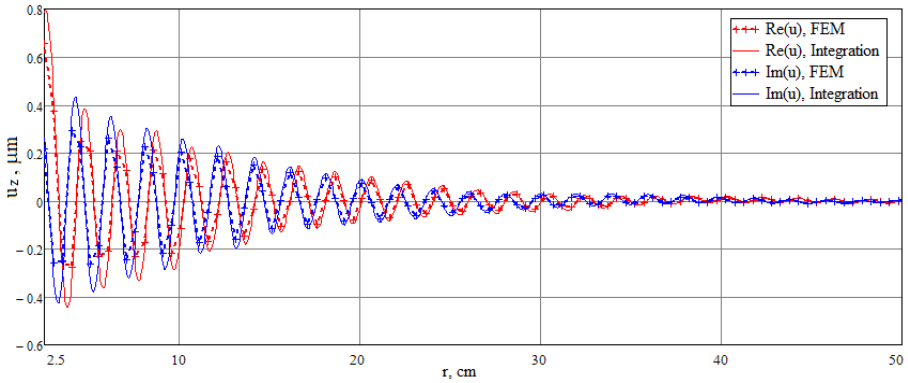

Fig. 15. Surface *z*-displacement of anisotropic plate at $\gamma = 0°$ and f=40 kHz

7. Conclusions

In this paper, an effect of an adhesive layer between an infinite 3D-layer and a piezoelectric actuator is analysed. Vibrations of the two host structures made of isotropic material and of carbon fibre plate excited by a circular piezoelectric actuator were investigated. A significant effect of the bonding layer on the resulting contact shear stresses was shown. A thicker adhesive layer produces the dumped load transfer between the PZT-element and the host structure. In the case when the bonding layer thickness is equal to zero, shear stresses concentrate near the end points of the contact area. It was shown that both *r*- and *z*- surface displacements are not strongly influenced by the thickness of the adhesive layer especially far from the contact zone. At the same time, the angle γ effects the distribution of the displacement fields in case of a composite plate. It is obvious that the *r*-components of displacements along the composite fibres take approximately ten times higher amplitudes than the displacements across the fibres, and approximately five times higher values for *z*-displacements.

Two approaches are used to simulate the excitation of the host structure: finite-element method and the semi-analytical approach based on the use of the Fourier transform. The resulting displacement fields, caused by a circular surface load, are compared for both approaches for anisotropic host structure at different vibration frequencies. Both applied methods showed a good agreement especially in a far field. The analysis of the obtained wave fields showed that both approaches can be effectively used for isotropic and composite structures at lower frequencies. For a growing vibration frequency, the FE-model of anisotropic plate needs a significant FE-mesh refinement and leads to considerable calculation times. It can be concluded that at higher frequencies the semi-analytical approach is preferable especially in case of composite host structures.

Acknowledgements. *This research was supported by the German Federal Ministry of Education and Research (BMBF), Grant No. 13FH009IX5.*

References

[1] Kalliomäki K. Condition Monitoring, Methods and a General Purpose Monitoring System. *IFAC Proceedings Volumes*. 1983;16(21): 295-304.
[2] Wechsler A, Mecrow BC, Atkinson DJ, Bennett JW, Benarous M. Condition monitoring of dc-link capacitors in aerospace drives. *IEEE Trans. Ind. Appl.* 2012;48(6): 1866-1874.
[3] Jolly MR, Prabhakar A, Sturzu B, Hollstein K, Singh R, Thomas S, Foote P, Shaw A. Review of Non-destructive Testing (NDT) Techniques and their applicability to thick walled composites. *Procedia CIRP*. 2015;38: 129-136.
[4] Giurgiutiu V. Tuned Lamb Wave Excitation and Detection with Piezoelectric Wafer Active Sensors for Structural Health Monitoring. *Intell. Mater. Syst. Struct.* 2005;16: 291-305.
[5] Raghavan A, Cesnik CES. Finite-dimensional piezoelectric transducer modeling for guided wave based structural health monitoring. *Smart Mater. Struct.* 2005;14: 1448-1461.
[6] Giurgiutiu V. *Structural Health Monitoring with Piezoelectric Wafer Active Sensors*. Elsevier: Academic Press; 2007.
[7] Salas KI, Cesnik CES. Guided wave structural health monitoring using CLoVER transducers in composite materials. *Smart Mater. Struct.* 2010;19: 015014.
[8] Karmazin A, Kirillova E, Seemann W, Syromyatnikov P. A study of time harmonic guided Lamb waves and their caustics in composite plates. *Ultrasonics*. 2013;53: 283-293.
[9] Glushkov EV, Glushkova NV, Evdokimov AA, Zhang CH. Guided wave Generation in Elastic Layered Substrates with Piezoelectric Coatings and Patches. *Physics Procedia.* 2015;70: 945-948.
[10] Islam MM, Huang H. Effects of adhesive thickness on the Lamb wave pitch-catch signal using bonded piezoelectric wafer transducers. *Smart Mater. Struct.* 2016;25: 085014.
[11] Sungwon Ha, Chang Fu-Kuo. Adhesive interface layer effects in PZT-induced Lamb wave propagation. *Smart Mater. Struct*. 2010;19: 025006.
[12] Nieuwenhuis JH, Neumann J, Greve DW, Oppenheim IJ. Generation and detection of guided waves using PZT wafer transducers. Ultrasonics, Ferroelectrics, and Frequency Control. *IEEE Trans. on Ultrasonics, Ferroelectrics, and Frequency Control.* 2005;52(11): 2103-2111.
[13] Kirillova E, Seemann W, Shevtsova M. Modeling the Interaction of Piezoelectric Actuators with Elastic Structures. In: Parinov IA, Chang SH., Jani MA. (eds.) *Advanced Materials Techniques, Physics, Mechanics and Applications*. Springer Proceedings in Physics book series (SPPHY, volume 193). Cham: Springer; 2017. p.501-510.
[14] Ostachowicz W, Kudela P, Malinowski P, Wandowski T. Damage localisation in plate-like structures based on PZT sensors. *Mech. Syst. and Signal Proc.* 2009;23: 1805-1829.
[15] Giurgiutiu V, Zagrai AN. Characterization of piezoelectric wafer active sensors. *J. Intell. Mater. Syst. Struct.* 2000;11: 959-976.
[16] Crawley E, Luis J. Use of Piezoelectric Actuators as Elements of Intelligent Structures. *AIAA J.* 1987;25: 1373-1385.
[17] Seshu P, Naganathan N. Finite-element analysis of strain transfer in an induced strain actuator. *Smart Mater. Struct.* 1997;6: 76-88.
[18] Sirohi J, Chopra I. Fundamental Understanding of Piezoelectric Strain Sensors. *J. Intell. Mater. Syst. Struct.* 2000;11: 246-257.
[19] Rabinovitch O, Vinson J. Adhesive Layer Effects in surface-mounted Piezoelectrics Actuators. *J. Intell. Mater. Syst. Struct*. 2002;13(11): 689-704.

[20] Han L, Wang XD, Sun Y. The effect of bonding layer properties on the dynamic behaviour of surface-bonded piezoelectric sensors. *Int. J. Solids and Struct*. 2008;45: 5599-5612.
[21] Bhalla S., Soh C. Electromechanical Impedance Modeling for Adhesively Bonded Piezo-Transducers. *J. Intell. Mater. Syst. Struct*. 2004;15: 955-972.
[22] Babeshko V, Glushkov E, Zinchenko Z. *Dynamics of Inhomogeneous Linearly Elastic Media.* Moscow: Nauka; 1989. (In Russian)
[23] Xu PC, Mal A. An adaptive integration scheme for irregularly oscillatory functions. *Wave Motion.* 1985;7: 235-243.